Physical Properties of Local Star-Forming Analogues to $z \sim 5$ Lyman Break Galaxies

Stephanie M. L. Greis[1⋆], Elizabeth R. Stanway[1], Luke J. M. Davies[2] & Andrew J. Levan[1]

[1] *Department of Physics, University of Warwick, Gibbet Hill Road, Coventry, CV4 7AL, UK*
[2] *ICRAR, The University of Western Australia, 35 Stirling Highway, Crawley, WA 6009, Australia*

Accepted yyyy Month dd. Received yyyy Month dd; in original form yyyy Month dd

ABSTRACT

Intense, compact, star-forming galaxies are rare in the local Universe but ubiquitous at high redshift. We interpret the 0.1-22 μm spectral energy distributions (SED) of a sample of 180 galaxies at $0.05 < z < 0.25$ selected for extremely high surface densities of inferred star formation in the ultraviolet. By comparison with well-established stellar population synthesis models we find that our sample comprises young ($\sim$ 60 - 400 Myrs), moderate mass ($\sim 6 \times 10^9\,\mathrm{M}_\odot$) star-forming galaxies with little dust extinction (mean stellar continuum extinction $E_{\mathrm{cont}}(B-V) \sim 0.1$) and find star formation rates of a few tens of Solar masses per year. We use our inferred masses to determine a mean specific star formation rate for this sample of $\sim 10^{-9}$ yr^{-1}, and compare this to the specific star formation rates in distant Lyman break galaxies (LBGs), and in other low redshift populations. We conclude that our sample's characteristics overlap significantly with those of the $z \sim 5$ LBG population, making ours the first local analogue population well tuned to match those high redshift galaxies. We consider implications for the origin and evolution of early galaxies.

Key words: galaxies: evolution – galaxies: high redshift – galaxies: star formation

1 INTRODUCTION

Massive nearby galaxies, including the one we currently inhabit, started their lives as low-mass, low-metallicity star-forming galaxies in the early Universe. Many of these smaller progenitors likely passed through a phase in which they appeared as Lyman break galaxies, named after a distinctive drop in their observed flux shortwards of their rest-frame

tween a pair of photometric filters. Steidel et al. (1996) developed the drop-out technique using *UGR* filters, thereby favouring the discovery of $z \sim 3-4$ LBGs, which drop out in the U-band. Since then many studies have been undertaken on both $z \sim 3$ LBGs and their local analogues. Direct observations of $z \sim 3$ LBGs reveal their rest-frame optical properties (e.g. Shapley et al. 2001), luminosity functions (e.g. van der Burg et al. 2010), UV-optical SEDs

В качестве аналогов далеких LBG (1<z<10) предлагались:

- highly ultraviolet-luminous starbursts at z ~ 0.1 – 0.2 (UVLGs)
- extreme optical emission line galaxies (EELS, EELGs or ‘Green Peas’ Cardamone et al. 2009;Amor´ın et al. 2015).
- the pilot sample identified by Stanway & Davies (2014): 21 compact star-forming galaxies in the local ($0.05 < z < 0.25$) Universe.

Выборка расширена до 180 candidate objects with $0.05 < z < 0.25$. This sample selects on ultraviolet properties and physical size (SDSS+GALEX).

- Выборка расширена до 180 candidate objects with $0.05 < z < 0.25$. This sample selects on ultraviolet properties and physical size (SDSS+GALEX).

UV colours satisfy $-0.5 < FUV - NUV < 0.5$ or

$-0.5 < FUV - r < 1.0$, where FUV and NUV correspond to the observed frame GALEX far- and near-ultraviolet bands at ~ 1500°A and ~ 2300°A.

Для SED использовались также ИК-данные по WISE.

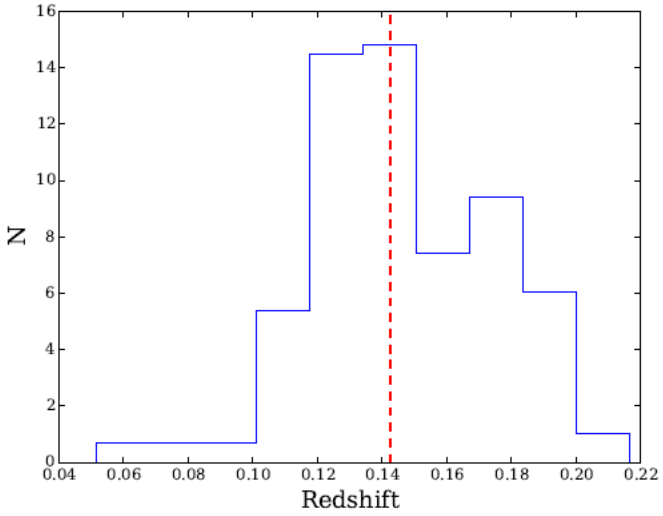

Figure 1. Distribution over redshift z of the sample of 180 candidate galaxies. The median redshift of $\sim$0.14 is indicated by the dashed vertical line.

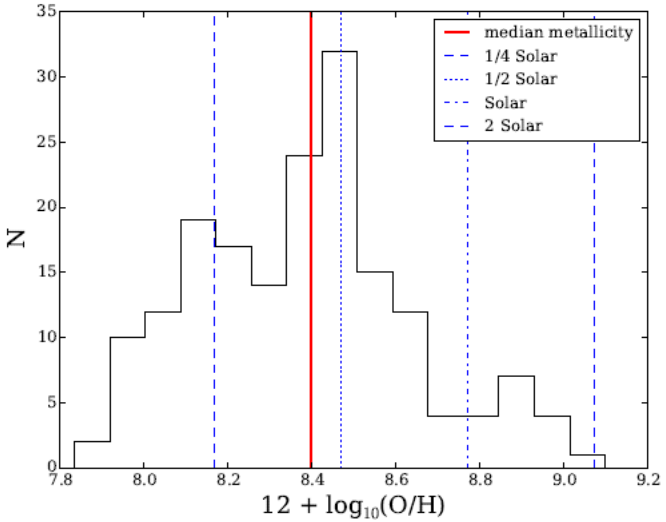

Figure 2. The oxygen abundance distribution of our sample as calibrated from strong emission line ratios in SDSS spectroscopy, using the line diagnostic of Dopita et al. (2016). Dashed vertical

- Модели: Matrason 2005 SFR~exp(-t/τ)
- BPASS models: The Binary Population and Spectral Synthesis code (Eldridge et al in prep). Учет эмиссии по Cloudy.
- Matrason+CIGALE fitting code (Burgarella, Buat, & Iglesias-P´aramo 2005;Roehlly et al. 2014). This incorporates stellar, nebular, and dust extinction components.

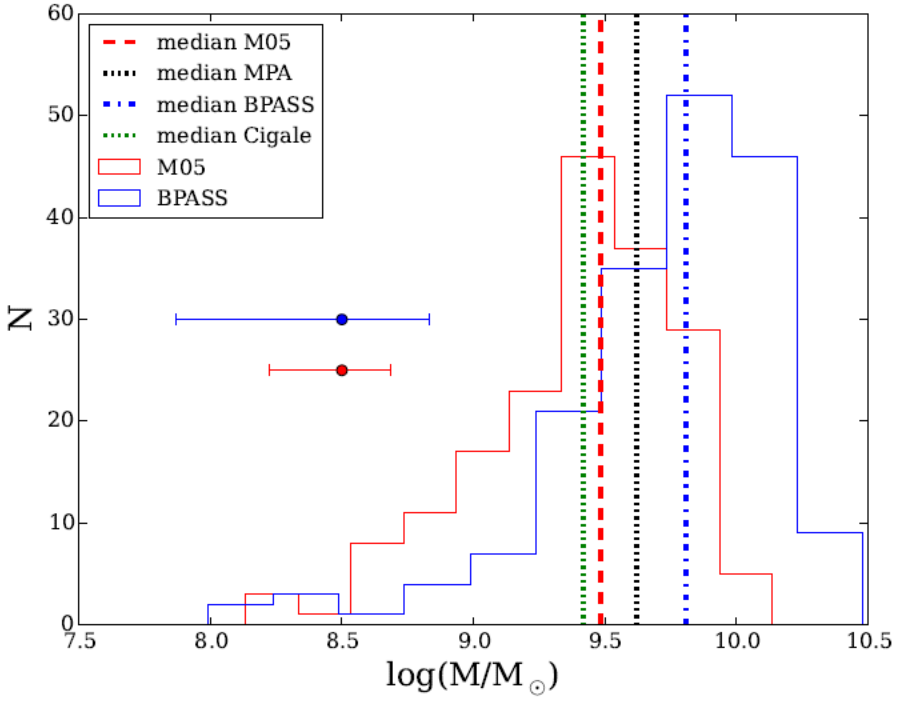

Figure 3. The distribution of derived stellar masses, comparing the M05 and BPASS models. The median fitted values are indicated by vertical dashed lines, as are those independently found by MPA-JHU and by fitting the data with the CIGALE code and M05 models. These all show good agreement. Representative

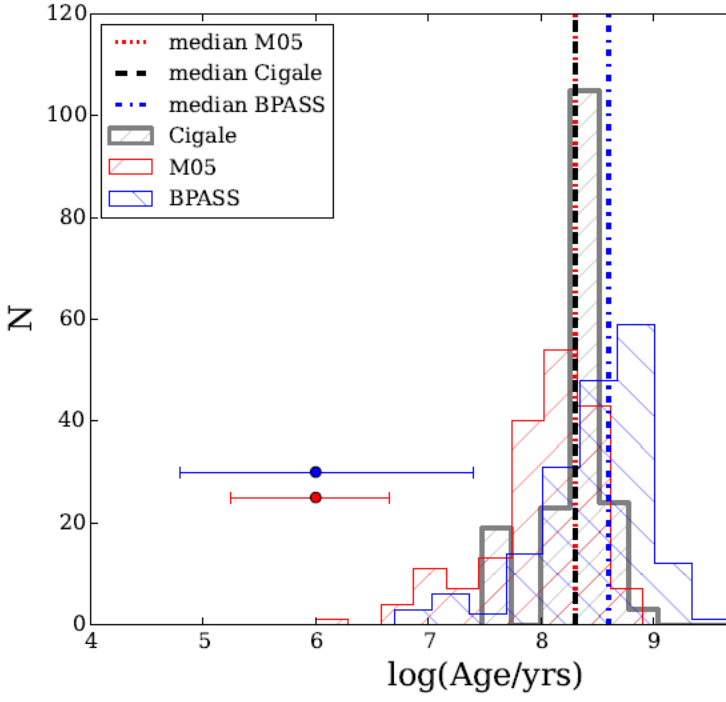

Figure 4. Distribution of the stellar population
get galaxies found using SED fitting with the M
models. Indicative uncertainty ranges on indivi
indicated by points.

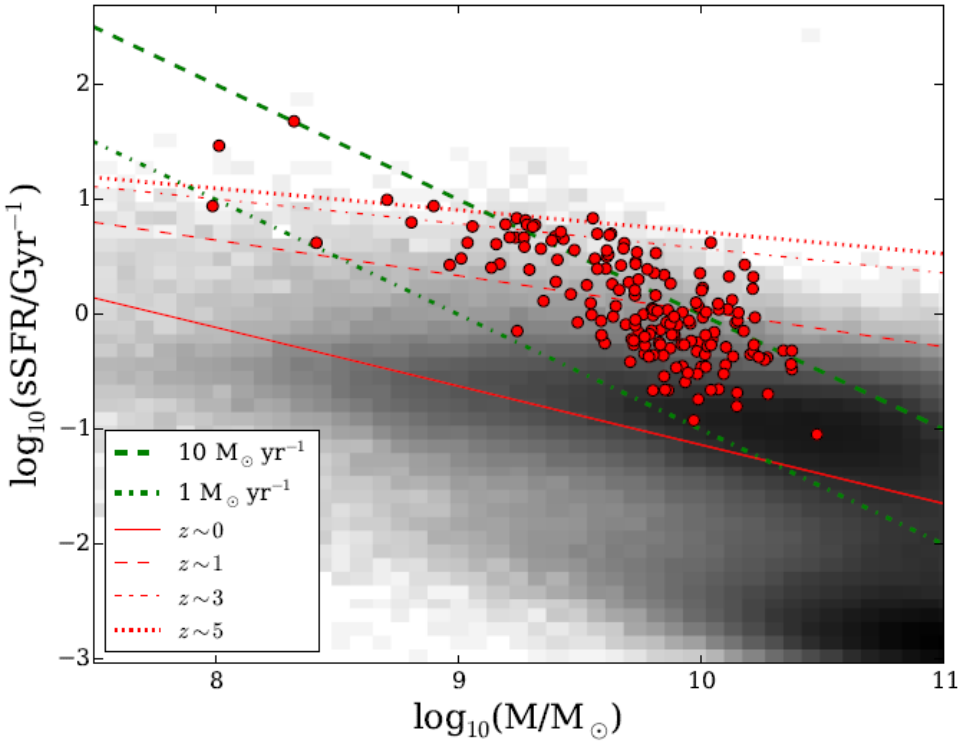

Figure 9. Specific star formation rate (as $\log_{10}(\mathrm{sSFR/Gyr^{-1}})$) vs mass of our sample (red dots), using the Hα SFR conversion. The green dashed and dot-dashed lines represent constant star formation rates of 10 $\mathrm{M_\odot\ yr^{-1}}$ and 1 $\mathrm{M_\odot\ yr^{-1}}$ respectively. The red lines represent the star formation main sequence at different redshifts according to Leslie et al. (2016). The underlying grey distribution gives the logarithm of the local SDSS galaxies' distribution. It is apparent that our objects lie significantly above the main sequence for local galaxies.

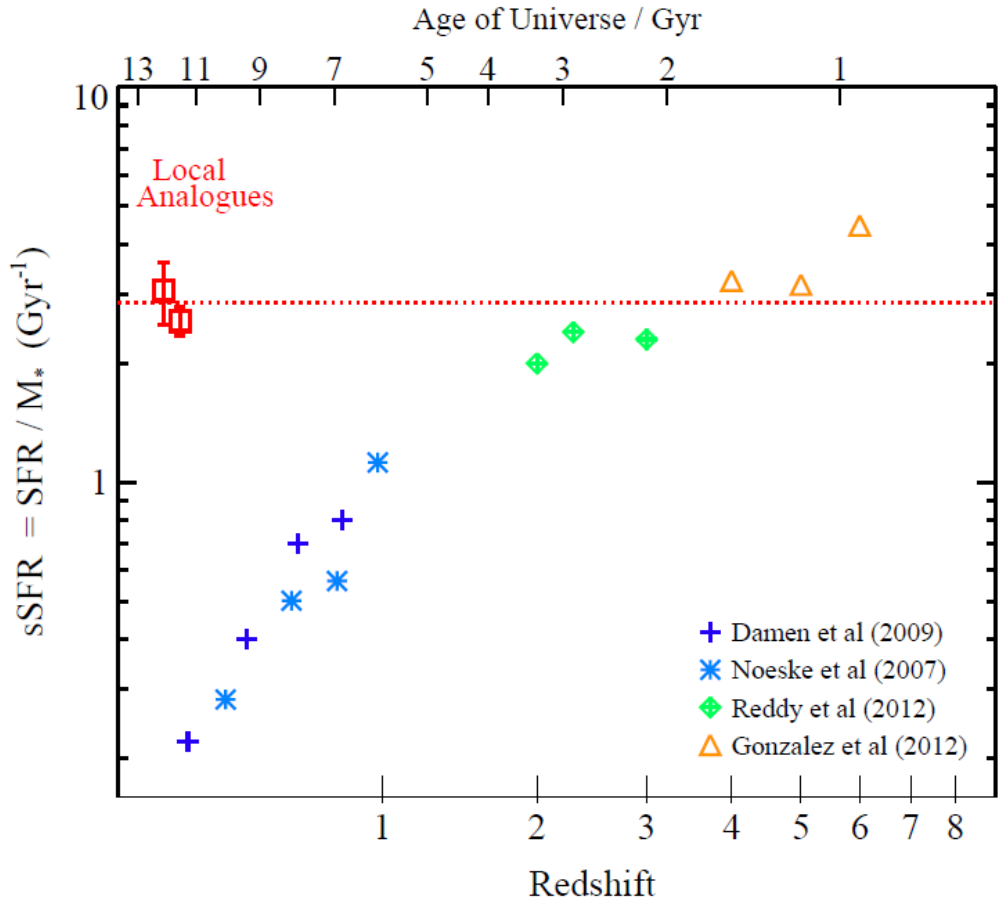

Figure 13. The specific star formation rate (sSFR) of our sample (red squares) compared to other galaxy populations at different redshifts. We split our sample into two redshift subsets, at $0.05 < z < 0.15$ and $0.15 < z < 0.25$, and indicate the mean of the entire sample with a dotted line. The average sSFR of our sample is significantly higher than that of other local and low-redshift galaxies, but in very good agreement with the sSFRs found for $4 < z < 6$ LBGs.

Основные выводы

- Выделена популяция галактик, по свойствам (SFR, M*, E(b-v)) не отличимая от LBGs на z~5
- Log M*~9.8, log age ~8.6, E(b-v)~0.12, SFR~(2.5 – 14) Mc/yr.

STAR CLUSTERS IN M31: VII. GLOBAL KINEMATICS AND METALLICITY SUBPOPULATIONS OF THE GLOBULAR CLUSTERS A-ph 1603.06947

- GC sample is based on high signal-to-noise spectra from the MMT/Hectospec (Fabricant et al.2005), which provide not only high-precision velocities (6 km/s), but also secure age and metallicity determinations from high signal-to-noise line indices.
- We have further added a small number of new observations of previously known clusters to the collection.

Metallicities were found by using iron dominated Lick indices as measured on Hectospec spectra.

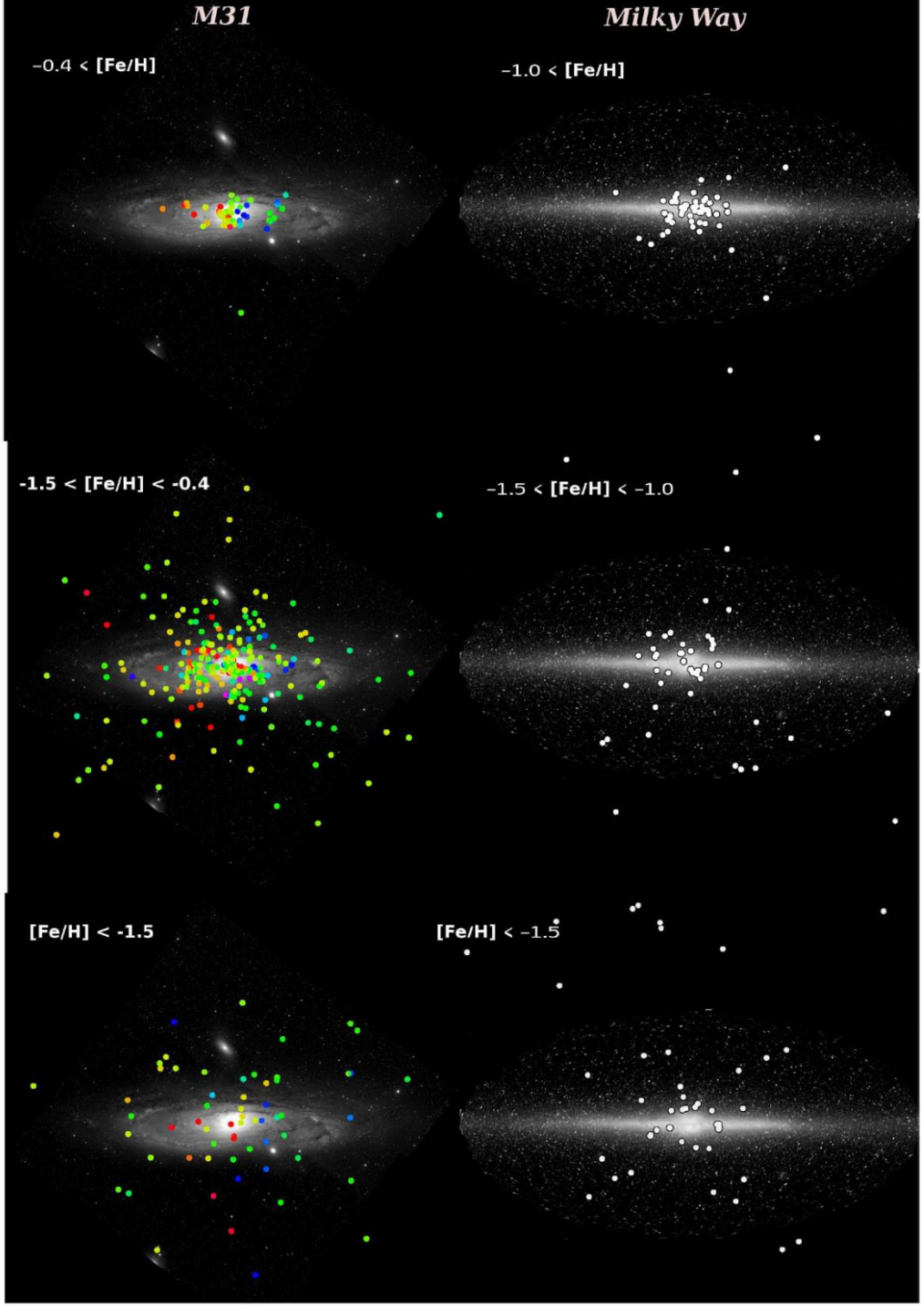

Caldwell, Romanowsky, 2016

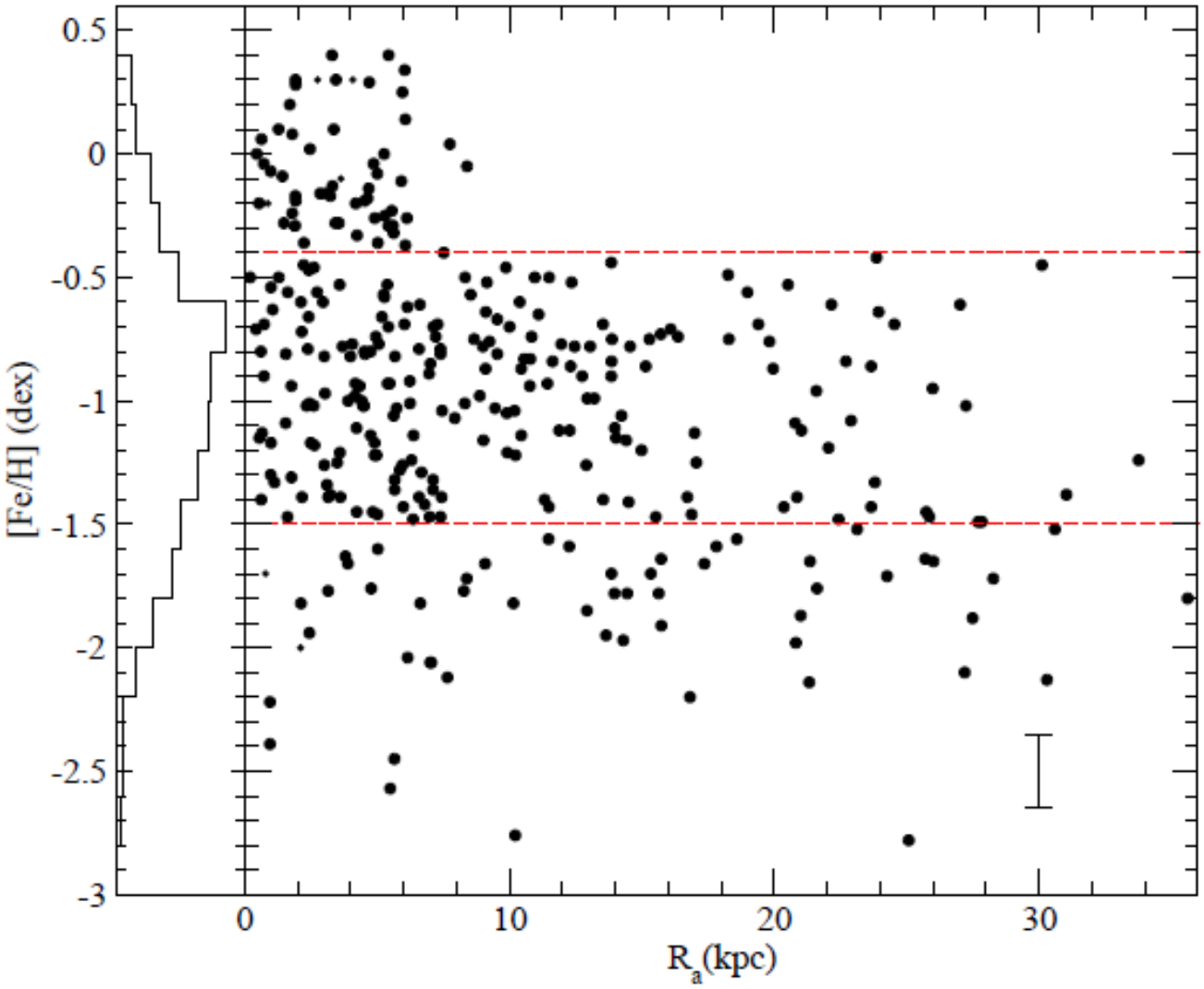

FIG. 1.— Distribution of M31 GC iron metallicity with semi-major axis radius, projected elliptically to the disk. In this plot, three metallicity groups emerge (with divisions at [Fe/H] ~ -0.4 and -1.5, shown as dashed lines), based on their relative densities inside and outside a disk radius of ~ 8 kpc. Note that eight clusters

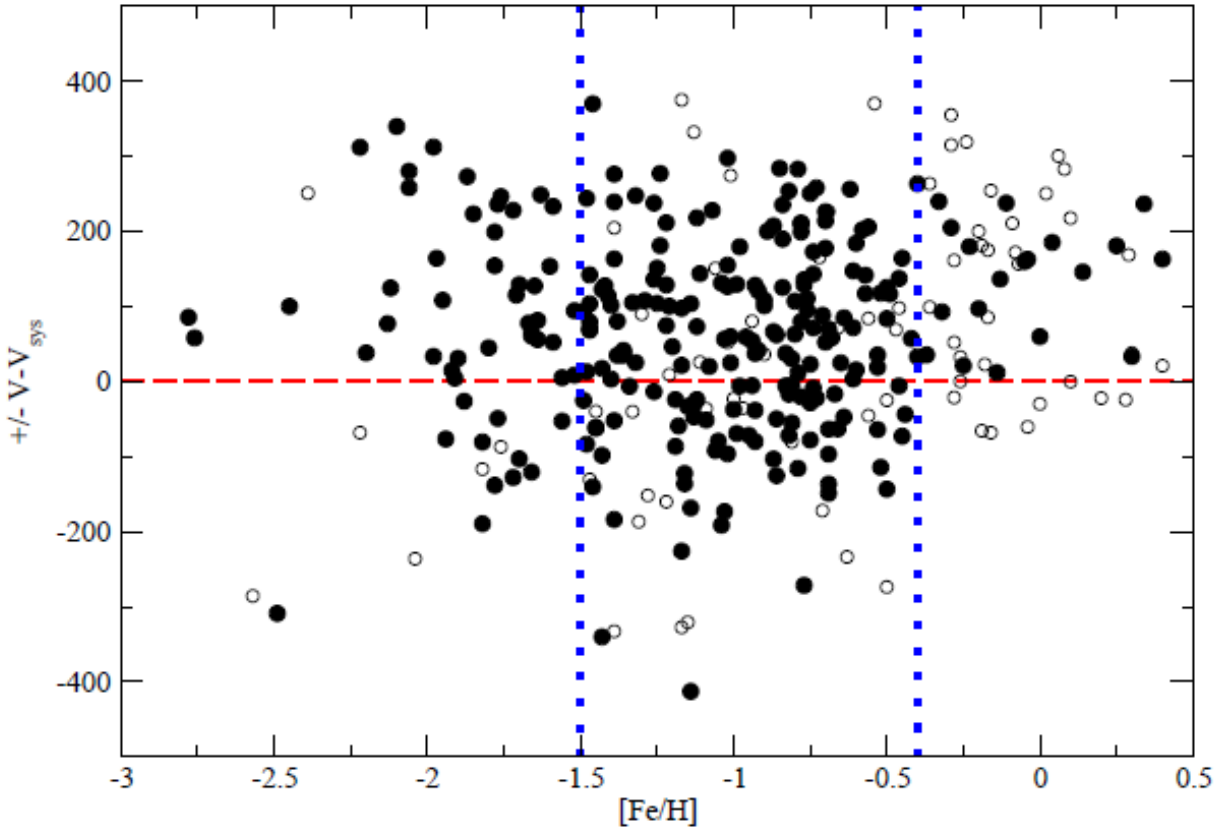

FIG. 2.— A second diagnostic plot outlining M31 GC metallicity groups. Here, velocity with respect to systemic velocity, with a sign inversion on opposite sides of the rotating disk, is plotted against [Fe/H]. Thus, objects with positive ordinate values are rotating prograde; retrograde velocities result in negative ordinate values. Clusters closer than 2 kpc to the center are shown as open circles; those farther out are shown as filled circles. This plot again suggests that clusters can be divided at [Fe/H]$= -0.4$ and [Fe/H]$= -1.5$, shown by the dotted vertical lines. Nearly all clusters more metal-rich than [Fe/H]$= -0.4$ have prograde motions. Lower metallicity clusters have roughly twice as many prograde as retrograde clusters, indicating systemic rotation for them.

Выводы по GCs in M31

- 1. В пределах оптических границ – вдвое больше GCs.
- Выделяются три группы GCs по металличности

✓ Metal-rich – за пределами балджа – это вращающийся диск! Внутреннее происхождение.

✓ Intermediate metal - очень слабое вращение

✓ Low metal - нет вращения, аналог GCs in MW